Journal for ImmunoTherapy of Cancer

Targeting *Gsk3a* reverses immune evasion to enhance immunotherapy in hepatocellular carcinoma

Xin Zheng ,[1] Luyu Yang,[1] Xiaotian Shen,[1] Junjie Pan,[1] Yiran Chen,[1] Jixuan Chen,[1] Hao Wang,[1] Jiaqi Meng,[2] Zhenchao Chen,[1] Sunzhe Xie,[1] Yitong Li,[1] Bolun Zhu,[1] Wenwei Zhu,[1] Lunxiu Qin,[1] Lu Lu[1]

To cite: Zheng X, Yang L, Shen X, *et al*. Targeting *Gsk3a* reverses immune evasion to enhance immunotherapy in hepatocellular carcinoma. *Journal for ImmunoTherapy of Cancer* 2024;**12**:e009642. doi:10.1136/jitc-2024-009642

► Additional supplemental material is published online only. To view, please visit the journal online (https://doi.org/10.1136/jitc-2024-009642).

XZ, LY, XS and JP contributed equally.

Accepted 30 July 2024

[1]Department of General Surgery, Hepatobiliary Surgery Center, Huashan Hospital & Cancer Metastasis Institute, Fudan University, Shanghai, China
[2]Third Affiliated Hospital of Naval Medical University, Shanghai, China

Correspondence to
Dr Lu Lu; lulu@huashan.org.cn

Lunxiu Qin; qinlx@fudan.edu.cn

Wenwei Zhu; westoolife@163.com

ABSTRACT

Background Immune escape is an important feature of hepatocellular carcinoma (HCC). The overall response rate of immune checkpoint inhibitors (ICIs) in HCC is still limited. Revealing the immune regulation mechanisms and finding new immune targets are expected to further improve the efficacy of immunotherapy. Our study aims to use CRISPR screening mice models to identify potential targets that play a critical role in HCC immune evasion and further explore their value in improving immunotherapy.

Methods We performed CRISPR screening in two mice models with different immune backgrounds (C57BL/6 and NPG mice) and identified the immunosuppressive gene *Gsk3a* as a candidate for further investigation. Flow cytometry was used to analyze the impact of *Gsk3a* on immune cell infiltration and T-cell function. RNA sequencing was used to identify the changes in neutrophil gene expression induced by *Gsk3a* and alterations in downstream molecules. The therapeutic value of the combination of *Gsk3a* inhibitors and anti-programmed cell death protein-1 (PD-1) antibody was also explored.

Results *Gsk3a*, as an immune inhibitory target, significantly promoted tumor growth in immunocompetent mice rather than immune-deficient mice. *Gsk3a* inhibited cytotoxic T lymphocytes (CTLs) function by inducing neutrophil chemotaxis. *Gsk3a* promoted self-chemotaxis of neutrophil expression profiles and neutrophil extracellular traps (NETs) formation to block T-cell activity through leucine-rich α-2-glycoprotein 1 (LRG1). A significant synergistic effect was observed when *Gsk3a* inhibitor was in combination with anti-PD-1 antibody.

Conclusions We identified a potential HCC immune evasion target, *Gsk3a*, through CRISPR screening. *Gsk3a* induces neutrophil recruitment and NETs formation through the intermediate molecule LRG1, leading to the inhibition of CTLs function. Targeting *Gsk3a* can enhance CTLs function and improve the efficacy of ICIs.

WHAT IS ALREADY KNOWN ON THIS TOPIC

⇒ The immunosuppressive microenvironment commonly present in hepatocellular carcinoma (HCC) is a major contributor to dysfunctional T cells. Immune checkpoint inhibitors have not led to improved therapeutic responses in patients with HCC.

⇒ Neutrophils are closely associated with the occurrence and progression of HCC. Neutrophils and neutrophil extracellular traps (NETs) released by them are critical for restricting T-cell function.

WHAT THIS STUDY ADDS

⇒ We identified and validated the immunosuppressive role of *Gsk3a* through CRISPR screen.

⇒ *Gsk3a* promotes neutrophil chemotaxis and NETs formation, leading to suppressed T-cell function.

⇒ *Gsk3a* affects leucine-rich α-2-glycoprotein 1 secretion via the nuclear factor kappa B/signal transducer and activator of transcription 3 (NFκB/STAT3) axis, thereby mediating changes in neutrophils.

⇒ Targeting *Gsk3a* effectively alleviated the immunosuppressive tumor microenvironment and sensitized tumors to anti-programmed cell death protein-1 therapy.

HOW THIS STUDY MIGHT AFFECT RESEARCH, PRACTICE OR POLICY

⇒ We provided novel perspectives on the immune evasion mechanisms of HCC, and *Gsk3a* may be a promising therapeutic target for immunotherapy in HCC.

INTRODUCTION

The innate and adaptive immune systems are essential for immune surveillance of cancer.[1] The interaction between the immune system and cancer cells is a continuous, dynamic, and intricate process.[2] Because of the unique physiological functions of the liver, hepatocellular carcinoma (HCC) cells possess an inherent advantage in immune evasion. The deactivation of cytotoxic T lymphocytes (CTLs) represents a crucial characteristic of HCC.[3] The function of CTLs is influenced by many factors in the tumor microenvironment (TME). In recent years, increasing evidence indicates that neutrophils can regulate T-cell function through direct or indirect mechanisms.[4–6] Moreover, neutrophil extracellular traps (NETs) released by neutrophils have been reported to alter the activation threshold of T cells.[7] However, the

role and mechanisms of neutrophils and NETs in mediating dysfunctional CTLs in HCC remain unclear.

HCC is the sixth most common cancer worldwide, with poor prognosis and high mortality rates because of its chemotherapy and radiotherapy resistance.[8] In recent years, immunotherapy represented by immune checkpoint inhibitors (ICIs) has revolutionized the treatment of a wide range of malignant tumors. ICIs have shown satisfactory results in clinical trials of various malignancies.[9–12] However, patients with HCC have a low overall response rate to ICIs, with only 20% and 17% of patients with advanced HCC responding to nivolumab and pembrolizumab, respectively, according to the results of two phase II clinical trials CheckMate-040 and KEYNOTE-224.[13 14] Therefore, uncovering the molecular mechanisms of how tumor cells evade immune cell killing is of great significance for improving the efficacy of immunotherapy and developing new immunotherapeutic strategies.

Due to its programmability and flexibility, CRISPR-mediated genome editing has become a powerful tool in cancer biology, and high-throughput screening methods based on its principle have become an effective means to search for new immune modulators and tumor immune targets.[15–18] Compared with in vitro, in vivo screening can better reflect the interaction between tumor cells and their immune microenvironment. In this study, using CRISPR screening, we identified *Gsk3a* as a critical candidate target for immune evasion in HCC. Functional and mechanistic studies demonstrated that *Gsk3a* could inhibit CTL activity by inducing neutrophil chemotaxis and NETs formation. Increased expression of *Gsk3a* was detected in anti-programmed cell death protein-1 (PD-1) antibody non-responsive patients. Pharmacological inhibition of *Gsk3a* could enhance CTL function and further improve the efficacy of anti-PD-1 antibody. In summary, our study provided new insights into the immune evasion mechanisms of HCC cells, and revealed *Gsk3a* may be a novel therapeutic target for immunotherapy in HCC.

MATERIALS AND METHODS

CRISPR sgRNA library and screen in vivo

A mouse disease-related immune gene library was screened, and the construction of the gene library was previously validated in a prior study. The gene library information used for screening is derived from the article by Ji *et al*.[18] The library consisted of 11,184 sgRNAs targeting 2,796 mouse genes corresponding to human diseases and the immune system, along with 816 non-targeting control sgRNAs. After synthesis and amplification of the DNA oligonucleotide library on a microarray, it was cloned into the lentiGuide-Puro vector to generate the disease-related immune gene library. The library was purified, and sequencing was performed to monitor the abundance changes of each sgRNA between the initial and final cell populations.

To generate cells with stable Cas9 expression, the lentiCas9-Blast (Addgene), pMD2.G (Addgene), and psPAX2 (Addgene) constructs were introduced into HEK 293 T cells for lentiviral packaging. Stable integrated Hepa1-6-Cas9 cells were selected using blasticidin (5 µg/mL). Cells infected with the virus containing the disease-related immune gene library were infected at a multiplicity of infection of 0.3 to ensure that each cell was infected with a single copy of the virus. After 48 hours of transduction, infected cells were selected with 5 µg/mL puromycin for 7 days. After 7 days, genomic DNA was extracted from a portion of the cells, while another portion was resuspended in phosphate-buffered saline (PBS) for transplantation. The transfected Hepa1-6-Cas9 cells containing the disease-related immune gene library were injected subcutaneously into C57BL/6 or NPG mice at a density of 4×10^6 cells per mouse for in vivo screening. The survival status of the mice and tumor size were monitored daily, and 2 weeks later, the mice were euthanized, and the tumors were dissected for further analysis.

The sgRNA sequences were amplified through two rounds of quantitative PCR (qPCR) and then subjected to sequencing using the HiSeq 2500 system (Illumina). The original FASTQ files were demultiplexed using Geneious V.8.0 (Biomatters). The constant regions of the sgRNA sequences were removed, and the read counts of each sgRNA per sample were normalized by the total read counts of each sample and subjected to logarithmic transformation. The MAGeCK analysis method was employed to quantify the abundance of sgRNAs in each sample. The proliferation-promoting and proliferation-inhibiting genes in C57BL/6 and NPG mice (n=5, each group) were ranked using robust rank aggregation (RRA), and key genes affecting immune adaptation were identified through cross-comparison. Please refer to online supplemental tables S1 and S2 for detailed information.

In vivo animal studies

To validate immune-related genes in vivo, subcutaneous xenograft models were established by injecting 4×10^6 different HCC cells subcutaneously into immunocompetent C57BL/6 mice and severely immunodeficient NPG mice (n=5, each group). Tumor volume was measured at intervals of 2–3 days when the subcutaneous tumors were macroscopically visible and calculated using the formula: Volume $=(\text{length}\times\text{width}^2)/2$. At the end of each experiment, mice were euthanized, and the tumors were dissected, weighed, and photographed. Subsequent immunofluorescence staining was performed after tumor fixation with 4% paraformaldehyde.

All animals were fed under standard conditions. The animal experiments were conducted in an specific-pathogen-free (SPF) grade laboratory and approved by the Animal Ethics Committee of Fudan University (2023-HSYY-295JZS, Shanghai, China).

The rest of the mouse studies are available in the online supplemental methods.

Flow cytometry analysis

Preparation of single-cell suspension: For flow cytometry of tumor cells in vivo, fresh mouse tumor tissue of appropriate size was dissected and mechanically separated using sterile ophthalmic scissors. The tumor fragments were then incubated at 37°C in serum-free Roswell Park Memorial Institute (RPMI) 1640 medium supplemented with DNase I (0.1 mg/mL; Solarbio), collagenase I (1 mg/mL; Sigma-Aldrich), collagenase II (1 mg/mL; Sigma-Aldrich), and collagenase IV (1 mg/mL; Sigma-Aldrich) for 60 min with continuous stirring. The resulting single-cell suspension was passed through a 70 µm cell strainer (Miltenyi). Subsequently, red blood cells within the tumor were lysed for 5 min using red blood cell lysis buffer (Miltenyi) at room temperature. The lysed tumor cells were then centrifuged at 400 g for 5 min at 4°C, and the reaction was stopped by adding 5% fetal bovine serum (FBS) RPMI 1640 medium. For flow cytometry experiments in vitro, the suspended immune cells in the lower chamber of a Transwell system were collected and washed three times with PBS before being collected in centrifuge tubes.

The cells were washed with PBS and stained with BD Horizon Fixable Viability Stain 510 (BD Biosciences) at a 1:1,000 dilution in PBS for 15 min at 4°C. Afterward, the cells were blocked with a monoclonal antibody against CD16/32 (BioLegend) at 4°C for 15 min. For surface staining, cells were stained with fluorescently labeled surface protein antibodies in a staining buffer at 4°C for 30 min. For intracellular staining (interferon-gamma (IFN-γ), granzyme B (GZMB) and forkhead box protein P3 (Foxp3)), cells were fixed and permeabilized after surface staining. Follow the manufacturer's instructions using Fix/Perm Buffer (BD, 562574) and Perm/Wash Buffer (BD, 562574) to fix and permeabilize the cells. After fixation and permeabilization, incubate the samples with the appropriate antibodies at 4°C for 30 min. The antibodies and concentrations used for staining are detailed in online supplemental table S3.

Flow cytometry data acquisition was performed using a CytoFLEX flow cytometer (Beckman Coulter), and data analysis was conducted using FlowJo software (V.10.8.1, TreeStar).

Human specimens

A cohort comprising 23 patients with HCC who underwent liver resection for primary onset was obtained from Huashan Hospital. According to the staging system for chronic liver disease, there were 16 cases in stages S0/1 and 7 cases in stage S4. The paraffin-fixed HCC tissues were obtained from 32 patients with HCC who underwent liver resection and received anti-PD-1 therapy at our institution. Response evaluation was performed every 3 months using the modified Response Evaluation Criteria in Solid Tumors. All samples were obtained in accordance with the Helsinki declaration, and written informed consent was obtained.

Statistical analysis

All data are presented as mean±SD. Statistical analysis was performed using Student's t-test or one-way analysis of variance. Correlation analysis was conducted using Pearson's correlation test. Survival data were analyzed using the Kaplan-Meier method and log-rank test. GraphPad statistical software (V.9.0) was used for all statistical analyses. Unless otherwise specified, all data were analyzed using two-tailed tests, and $p<0.05$ was considered statistically significant.

A detailed description of the methods used in this study is found in the online supplemental methods.

RESULT

CRISPR screening identified *Gsk3a* as a critical gene for immune evasion of HCC

To identify key genes regulating immune adaptability in HCC, we constructed an immune-related gene library consisting of 12,000 sgRNAs targeting 2,796 genes. The Hepa1-6 cells transduced with the library were, respectively, subcutaneously implanted into C57BL/6 (immunocompetent) and NPG mice (immunodeficient). After 2 weeks, the tumors were harvested from mice and subjected to high-throughput sgRNA sequencing (figure 1A). To reduce errors and improve the accuracy of the results, we excluded two samples because of low quality in next-generation sequencing (online supplemental figure S1A,B). Before implantation (day 0), the library expression of tumor cells followed a log-normal distribution. After implantation, significant changes in sgRNA expression were observed in the tumor tissues from both C57BL/6 and NPG mice models (online supplemental figure S1C). We ranked the negative selection scores obtained by the MAGeCK RRA algorithm after normalization. A normalized score >2 in the negative selection was defined as a promoting factor (figure 1B). The genes that could promote growth in both NPG and C57BL/6 mice were considered as oncogenes (red), while those that could only promote growth in C57BL/6, but not in NPG, were considered as immune evasion genes (blue) (figure 1C). Finally, we identified and characterized functionally important molecular targets for immune evasion in HCC cells (online supplemental table S2).

We conducted STRING analysis on the gene set associated with immune evasion and employed the Molecular Complex Detection (MCODE) plugin to identify core regulatory genes (figure 1D). Given that our screening was performed at the mouse genome level, we further wanted to explore whether these genes were significantly altered at the level of human transcription and protein expression. Five genes (*GSK3A*, *GRB2*, *MAVS*, *IRAK1*, *ILK*) were selected for further investigation, which were validated to be overexpressed in the human HCC from The Cancer Genome Atlas (TCGA) transcriptome and The Human Protein Atlas proteome, and associated with a worse prognosis (figure 1E,F and online supplemental figure S1D). Immuno-estimation indicated a close

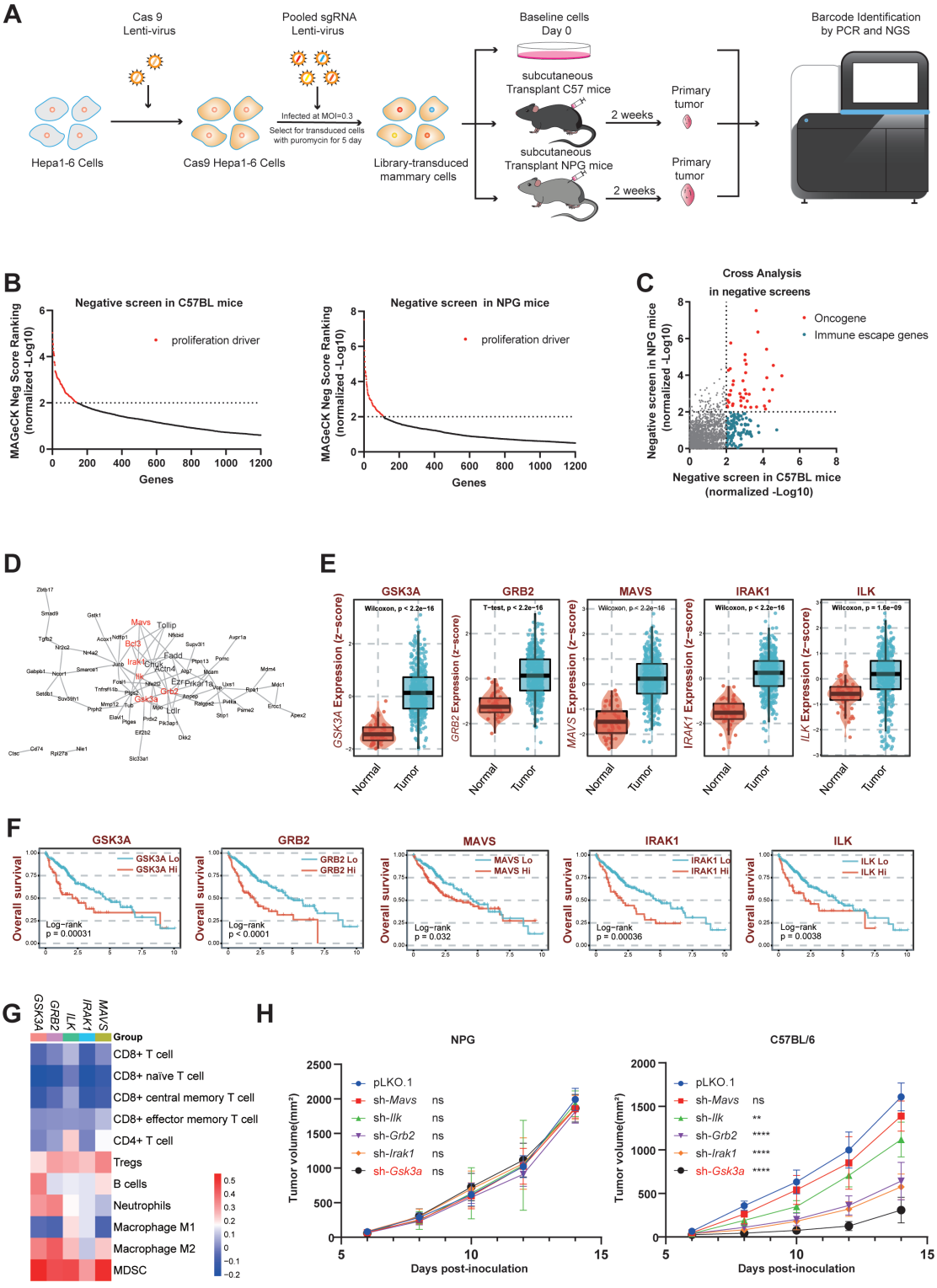

Figure 1 CRISPR screening identified *Gsk3a* as a critical gene for tumor immune evasion. (A) CRISPR in vivo screening schematic diagram. (B) Negative selection analysis of sgRNA abundance in transplanted tumors and control cells. Normalized score >2 was defined as a promoting factor. (C) Based on cross-validation analysis of negative selection in NPG mice and C57BL/6 mice, a group of oncogenes (red) and immune evasion genes (blue) can be identified. (D) STRING+MCODE identified core regulatory molecules in the interaction-regulated network of the immune evasion gene set. (E) Bar charts depicting the messenger RNA expression levels of *GSK3A*, *GRB2*, *MAVS*, *IRAK1*, and *ILK* in the TCGA database. (F) Overall survival analysis of *GSK3A*, *GRB2*, *MAVS*, *IRAK1*, and *ILK* expression in patients with liver cancer using TCGA database. (G) Correlation heatmap of *GSK3A*, *GRB2*, *MAVS*, *IRAK1*, and *ILK* expression with immune cell infiltration in the TIMER database. (H) Growth curves of stable knockdown cell lines of different genes in subcutaneous xenografts of C57BL/6 (n=5) and NPG mice (n=5). Data were presented as means±SD. **p<0.01; ****p<0.0001; ns, p≥0.05. MDSC, myeloid-derived suppressor cell; TIMER, Tumor Immune Estimation Resource; TCGA, The Cancer Genome Atlas; Treg, regulatory T cells.

relationship between the five enriched genes and altered immune cells component in the TME (figure 1G). We then knocked down the five genes with shRNA in murine HCC Hepa1-6 cells and adopted the subcutaneous implantation tumor models in mice of different immune-background, and confirmed varying degrees of growth inhibition only in immunocompetent C57BL/6 mice, but not immunodeficient NPG mice (figure 1H and online supplemental figure S2A–C). Among them, interfering *Gsk3a* exhibited the most significant inhibitory effect on tumor growth. Taken together, these findings indicate that *Gsk3a* is a critical gene for immune evasion of HCC.

The immune evasion effects of *Gsk3a* required the involvement of the tumor immune microenvironment

We then knocked-down (KD) or overexpressed (OE) *Gsk3a* in Hepa1-6 cells (sh-*Gsk3a* or *Gsk3a*-OE), and confirmed an impaired or increased tumor growth only in immunocompetent C57BL/6 mice (online supplemental figure S3A–C). In line with the unaltered tumor growth within an immunodeficient background, *Gsk3a* KD or OE also affected no proliferation, migration or apoptotic capacity of Hepa1-6 cells in vitro (figure 2A–C).

We then assessed the difference of immune cells component in TME between murine tumor of Hepa1-6 sh-*Gsk3a* and control (pLKO.1) by flow cytometry. Only neutrophils (Gr^+Ly6g^+) were significantly decreased in the sh-*Gsk3a* group. There was no changes in the infiltration of the other immune cells, such as T cells ($CD4^+$ and $CD8^+$), myeloid-derived suppressor cells (MDSCs) (Gr^+Ly6g^-), macrophages ($CD11b^+F4/80^+$), B cells ($CD45^+B220^+$), natural killer (NK) cells ($CD45^+NK1.1^+$), or regulatory T cells (Tregs) ($CD25^+Foxp3^+$) (figure 2D and online supplemental figure S4A–D). Despite that the total number of T cells was not affected (figure 2E), a higher proportion of functional T cells (IFN-γ^+CD8^+ and $GZMB^+CD8^+$) companied with a conversely decreased exhausted T cells (PD-1^+ and $LAG3^+$) was observed in the sh-*Gsk3a* group compared with the control (figure 2F–I). The results suggested that *Gsk3a* KD enhanced the cytotoxic function of CTLs, but this was independent of altering the ratio of T-cell populations. Immunofluorescence also confirmed a positive correlation between *Gsk3a* expression and neutrophils along with a negative correlation between *Gsk3a* and effector T cells, respectively (figure 2J). These results uncovered an altered TME by *Gsk3a* with a reverse change of infiltrated neutrophils and functional T cells.

Gsk3a inhibited T-cell function by inducing neutrophil infiltration and chemotaxis

To assess how *Gsk3a* reforms the immunosuppressive TME, we established an in vitro co-culture system consisting of $CD8^+$ T cells and neutrophils either alone or in combination in upper chamber, and Hepa1-6 cells in lower chamber, in which T-cell killing efficiency and leukocyte chemotaxis were observed simultaneously. The tumor-killing efficiency of T cells alone was not affected by *Gsk3a* KD, indicating that tumorous *Gsk3a* did not act directionally on T cells. However, when neutrophils were added, Hepa1-6 cells exhibited enhanced resistance to T-cell cytotoxicity, and this was impaired by *Gsk3a* KD (figure 3A). *Gsk3a* KD also reduced the tumor cells' ability to recruit neutrophils without affecting T cells recruitment (figure 3B,C). Flow cytometry analysis revealed no significant difference in the proportion of functional T-cell subsets between Hepa1-6 sh-*Gsk3a* and the control group when T cells were added alone. However, when neutrophils were added to T cells, the proportion of functional T-cell subsets decreased in both, but less in the sh-*Gsk3a* group (figure 3D,E). For validation, we repeated the co-culture system using human T cells, neutrophils and two common human HCC cell lines Hep3B and MHCC-97H with different GSK3A level (online supplemental figure S5A), and observed consistent changes in neutrophil chemotaxis and cytotoxic T-cell killing efficiency after intervening *GSK3A* in corresponding human cell lines (online supplemental figure S5B–D).

Consistently, depleting neutrophils by α-Ly6g abrogated the promoting effects of *Gsk3a*-OE Hepa1-6 cells on tumor growth in vivo (figure 3F,G). Depleting neutrophils did not affect $CD8^+$ T-cell infiltration but increased the proportion of functional T cells in the TME (figure 3H–J). These findings suggest that neutrophils play a critical role in mediating the *Gsk3a*-induced suppressive TME in HCC.

Tumor cells with altered *Gsk3a* expression can affect neutrophil self-chemotaxis and NETs formation

We conducted RNA sequencing (RNA-seq) on neutrophils treated with conditioned media (CM) from sh-*Gsk3a* or *Gsk3a*-OE Hepa1-6 cells to investigate how neutrophils are reshaped by tumorous *Gsk3a,* and found a significant change with 1,731 genes upregulated and 1,990 genes downregulated (online supplemental figure S6A). Gene Ontology analysis showed enrichment of inflammatory activation-related gene sets, including inflammatory response, neutrophil chemotaxis, and response to oxidative stress (online supplemental figure S6B). Notably, the neutrophil chemotaxis gene set was enriched, suggesting a potential self-amplifying chemotactic effect induced by *Gsk3a* (figure 4A and online supplemental figure S6B). We validated the upregulation of chemotactic genes (*Cxcl1*, *Cxcl2*, *Cxcl3*) in neutrophils with *Gsk3a*-OE Hepa1-6 cells CM (figure 4B). Neutrophils treated with CM from *Gsk3a*-OE Hepa1-6 cells exhibited enhanced recruitment compared with that from sh-*Gsk3a* ones (figure 4C).

Tumor-associated neutrophils (TANs) display diversity and can be categorized as antitumor (N1) or protumor (N2) phenotypes, but *Gsk3a* did not bias neutrophils toward neither N1 nor N2 (online supplemental figure S6C). However, Nos2, a key encoding nitric oxide synthase involved in NETs formation, was upregulated (online supplemental figure S6D).[19] Indeed, tumorous *Gsk3a* increased NETs-related genes expression in neutrophils (figure 4D). Consistently, CM from murine or human HCC cells with sh-*Gsk3a* and *Gsk3a*-OE impaired

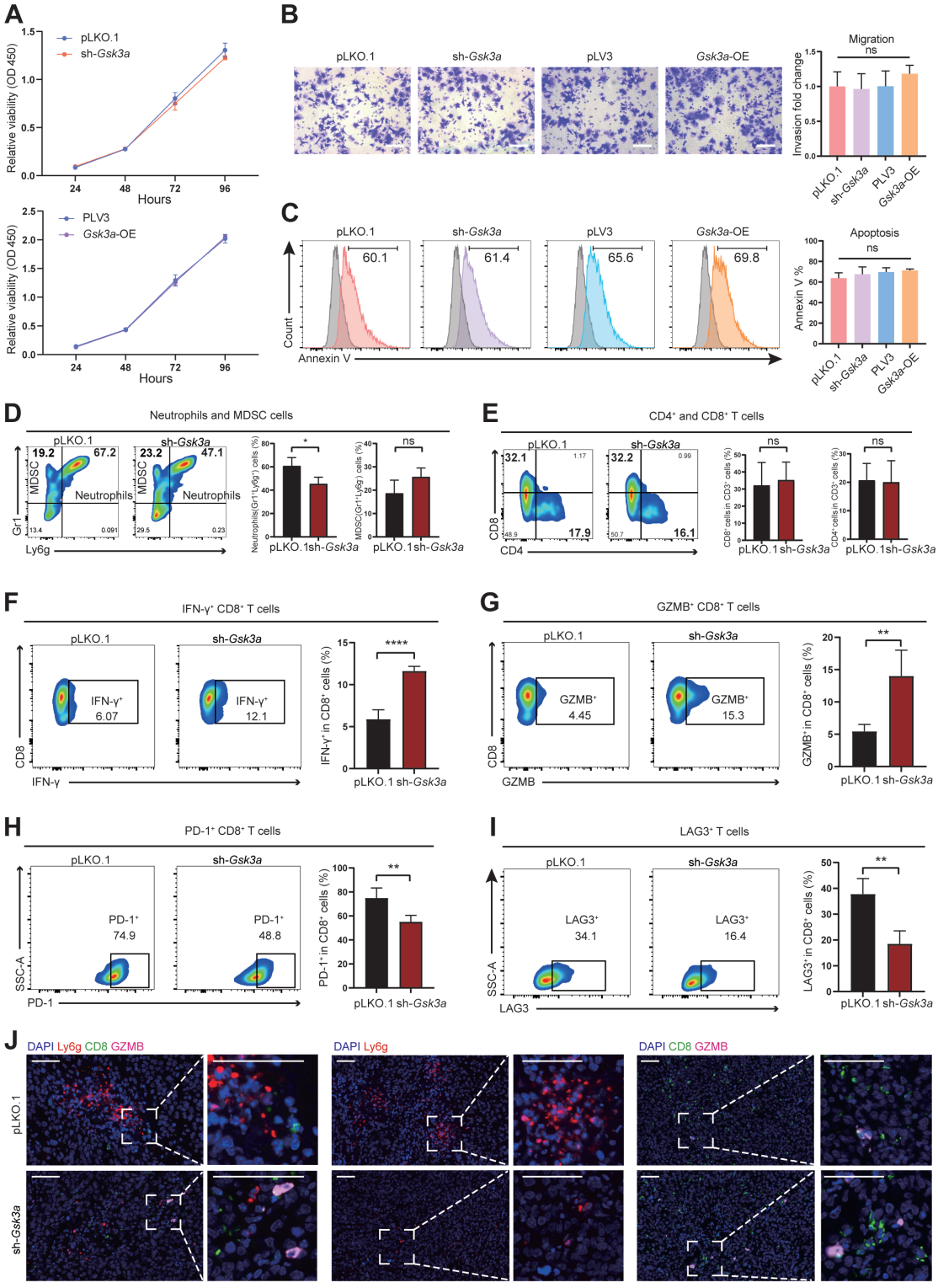

Figure 2 *Gsk3a* is associated with neutrophil infiltration and T-cell functional suppression. (A) In vitro cell growth curve of sh-*Gsk3a* or *Gsk3a*-OE Hepa1-6 cells. (B) Representative Transwell images showing the migration of sh-*Gsk3a* or *Gsk3a*-OE Hepa1-6 cells. (C) Representative histogram of annexin V positive sh-*Gsk3a* or *Gsk3a*-OE Hepa1-6 cells. (D–E) Representative images and bar plots of the percentage of immune cells in the tumor immune microenvironment analyzed by flow cytometry. For (D) Percentage of MDSC ($Gr1^+Ly6g^-$) and neutrophils ($Gr1^+Ly6g^+$) in the microenvironment. For (E) Percentage of $CD4^+$ and $CD8^+$ T cells in the microenvironment. (F–I) Flow cytometric analysis of the frequency of IFN-γ^+ cells in $CD8^+$ T cells (F) $GZMB^+$ cells in $CD8^+$ T cells (G) PD-1^+ cells in $CD8^+$ cells (H) and $LAG3^+$ cells in $CD8^+$ cells (I) isolated from TILs. (J) Representative immunofluorescence staining of $CD8^+$ T-cell (green), $GZMB^+$ cells (pink) and neutrophils (red) in vector controls and sh-*Gsk3a* Hepa1-6 tumors. Scare bar: 50 µm. All data were presented as means±SD. *p<0.05; **p<0.01; ****p<0.0001; ns, p≥0.05 MDSC, myeloid-derived suppressor cell; GZMB, granzyme B; IFN-γ, interferon-gamma; KO, knocked-down; MDSC, myeloid-derived suppressor cell; OE, overexpressed; PD-1, programmed cell death protein-1; TILs, tumor infiltrating lymphocytes.

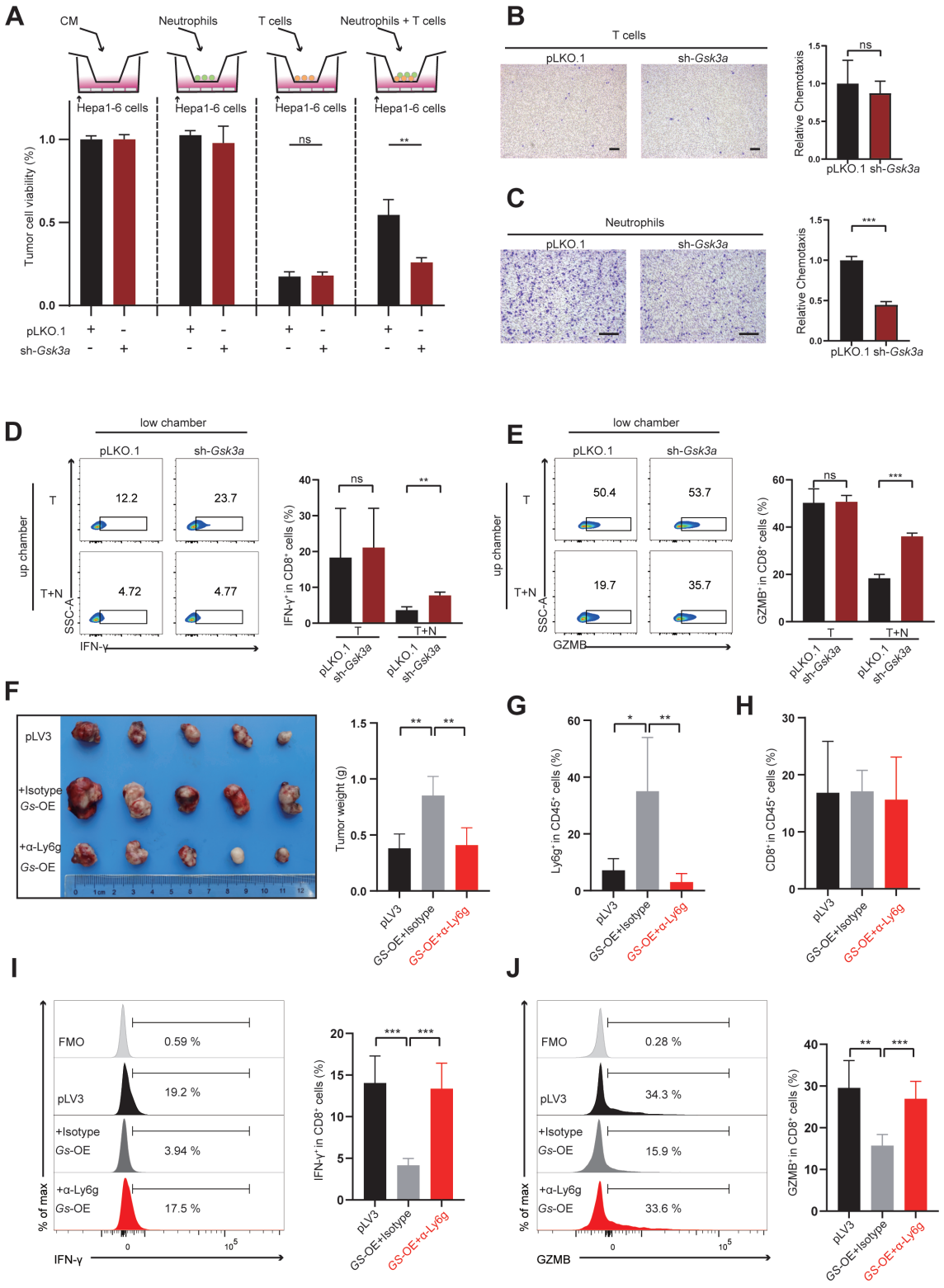

Figure 3 *Gsk3a* inhibits T-cell function by inducing neutrophil chemotaxis. (A–E) In vitro chemotaxis co-culture cytotoxicity experiment. In vitro co-culture cytotoxicity system schematic and bar graphs depicting the survival of underlying tumor cells measured by CCK-8 assay (A). Crystal violet staining of the Transwell membrane in the co-culture cytotoxicity system shows the chemotaxis of $CD8^+$ T cells (B) and neutrophils (C). Scare bar: 100 µm. Flow cytometric analysis of the frequency of IFN-γ^+ cells in $CD8^+$ T cells (D) and $GZMB^+$ cells in $CD8^+$ T cells (E) harvested from the lower chamber. (F) Tumor weight and images of transplanted *Gsk3a*-OE Hepa1-6 cells in C57BL/6 mice following the treatment of α-Ly6g or isotype antibody (n=5). (G–H) Flow cytometric analysis of the frequency of neutrophils (G) and $CD8^+$ T cells (H) from tumor immune microenvironment. (I–J) Flow cytometric analysis of the frequency of IFN-γ^+ cells in $CD8^+$ T cells (I) and $GZMB^+$ cells in $CD8^+$ T cells (J) from tumor immune microenvironment. All data were presented as means±SD. *p<0.05; **p<0.01; ***p<0.001; ns, p≥0.05. CM, conditioned media; GZMB, granzyme B; IFN-γ, interferon-gamma; KO, knocked-down; OE, overexpressed.

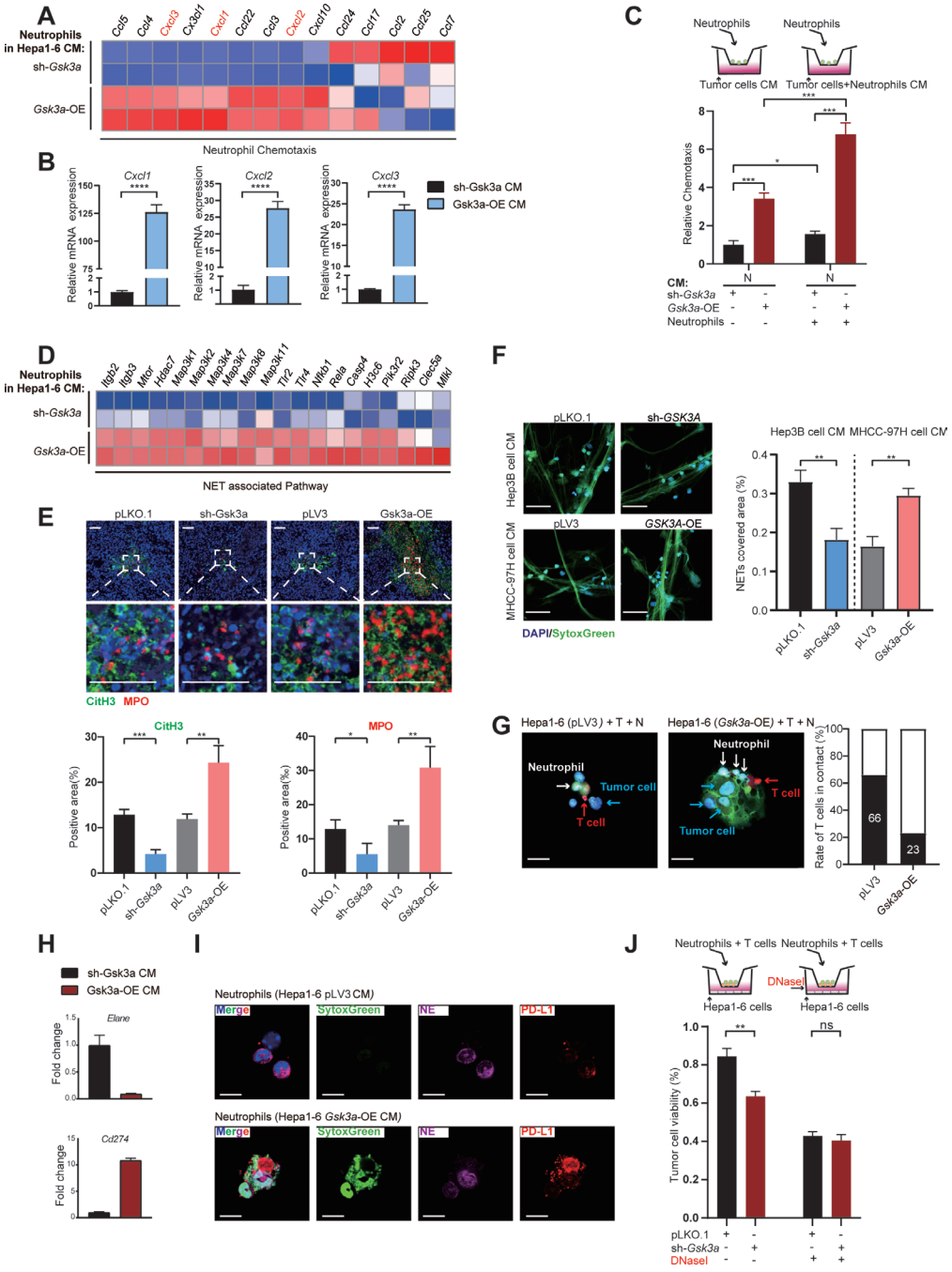

Figure 4 Tumor cells with altered *Gsk3a* expression can affect neutrophil self-chemotaxis and NETs formation. (A) The heatmap shows an upregulated expression of the neutrophil chemotaxis gene set in neutrophils cultured with CM from *Gsk3a*-OE Hepa1-6 cells. (B) *Cxcl1*, *Cxcl2* and *Cxcl3* mRNA in murine neutrophils co-cultured with sh-*Gsk3a* and *Gsk3a*-OE Hepa1-6 cells for 24 hours were analyzed by qPCR. (C) Migration of murine neutrophils recruited by CM from sh-*Gsk3a* or *Gsk3a*-OE Hepa1-6 cells, or from neutrophils pretreated with indicated Hepa1-6 CM. (D) The heatmap shows an upregulated expression of NETs associated pathway gene set in neutrophils cultured with CM from *Gsk3a*-OE Hepa1-6 cells. (E) Representative immunofluorescence staining of NETs (labeled in CitH3) and neutrophils (labeled in MPO) in sh-*Gsk3a* or *Gsk3a*-OE Hepa1-6 tumors. Scare bar: 50 µm. (F) Representative immunofluorescence staining of NETs (labeled in SytoxGreen) and DNA (labeled in DAPI) in neutrophils cultured with Hep3B and MHCC-97H cells CM in vitro. Scare bar: 50 µm. (G) Representative immunofluorescence images demonstrate NETs (labeled in SytoxGreen) enveloping tumor cells (labeled in DAPI and >10 µm), impeding their contact with T cells (labeled in Dil). Scare bar: 20 µm. (H) Bar plots show the expression of *Cd274* and *Elane* in RNA sequencing. (I) Representative immunofluorescence images show the expression of PD-L1 and NE within neutrophil-NETs structures. Scare bar: 10 µm. (J) The cell viability of pLKO.1 and sh-*Gsk3a* Hepa1-6 cells in the co-culture system with neutrophils and CD8$^+$ T cells was assessed using the CCK-8 assay, with or without DNase I treatment. All data were presented as means±SD. *p<0.05; **p<0.01; ***p<0.001; ****p<0.0001; ns, p≥0.05.CM, conditioned media; KO, knocked-down; mRNA, messenger RNA; NE, neutrophil elastase; NET, neutrophil extracellular trap; OE, overexpressed; PD-L1, programmed death-ligand 1; qPCR, quantitative PCR.

or increased NETs formation from homologous neutrophils in vitro, respectively. And this was also confirmed by increased NETs formation in sh-*Gsk3a* or *Gsk3a*-OE Hepa1-6 subcutaneous tumors in vivo (figure 4E,F and online supplemental figure S6E). Our previous studies have demonstrated the crucial role of NETs in promoting HCC metastasis.[20] To further illustrate how NETs contribute to immune invasion, we co-cultured neutrophils with *Gsk3a*-OE Hepa1-6 cells followed by T cells challenge to allow NETs formation, and found *Gsk3a*-induced NETs encasing tumor cells, hindering their interaction with cytotoxic CD8$^+$ T cells (figure 4G). Moreover, RNA-seq and immunofluorescence staining revealed that NETs induced by *Gsk3a*-OE CM were equipped with elevated programmed death-ligand 1 (PD-L1) and less cytotoxic neutrophil elastase (NE),[21] which further enhanced the immunosuppressive capacity (figure 4H,I). Finally, DNase I treatment degraded NETs, effectively rescuing the impaired tumor cells killing efficiency of T-cell induced by tumorous *Gsk3a* (figure 4J). We observed the same effect in human cell lines (online supplemental figure S6F).

Gsk3a promotes recruitment and NETs formation of neutrophil through leucine-rich α-2-glycoprotein 1

To investigate cellular communication of how tumorous *Gsk*3a impact neutrophils, we performed RNA-seq on sh-*Gsk3a* and pLKO.1 Hepa1-6 cells. We found that the expression of secreting factor *Lrg1* was most significantly downregulated in sh-*Gsk3a* cells (figure 5A). Interestingly, classic neutrophil and immune cell chemokines exhibited no significant changes (online supplemental figure S7A). To confirm the correlation between *Gsk3a* and *Lrg1* expression, we quantified *Lrg1* expression intracellularly and extracellularly using qPCR and ELISA, showing reduced *Lrg1* expression with *Gsk3a* (figure 5B,C). Moreover, the protein expression of leucine-rich α-2-glycoprotein 1 (LRG1) was also downregulated both in murine and human HCC cells by western blot (online supplemental figure S7B,C). Consistently, it was further confirmed that *Lrg1* was induced by *Gsk3a* through transcription factors nuclear factor kappa B (NFκB) and signal transducer and activator of transcription 3 (STAT3) (figure 5D).[22 23] *Lrg1* has been reported to induce neutrophil chemotaxis and amplify the effect through autocrine secretion.[24] To our expectation, in vitro addition of recombinant LRG1 restored the expression of neutrophil self-amplifying chemokines reduced in neutrophils treated with sh-*Gsk3a* CM (figure 5E). The impaired neutrophils chemotaxis and NETs formation after interfering *Gsk3a*/*GSK3A* in murine Hepa1-6 and human Hep3B cells were also restored by LRG1 (figure 5F,G and online supplemental figure S7D,E). In the HCC cells-T cells-neutrophils co-culture system, LRG1 addition restored the impaired survival of sh-*Gsk3a* tumor cells to the control level, which was nullified by DNase I digestion of NETs (figure 5H and online supplemental figure S7F). Flow cytometry analysis of CD8$^+$ T cells transmigrating into the lower chamber revealed that LRG1 reduced the proportion of cytotoxic T cells (IFN-γ$^+$CD8$^+$T cell and GZMB$^+$CD8$^+$T cell), which was reversed by DNase I (figure 5I). In vivo, the addition of LRG1 increased tumor volume and weight of sh-*Gsk3a* tumors, which was counteracted by DNase I co-administration (figure 5J). DNase I reversed T-cell function inhibited by LRG1, while the increased the neutrophils infiltration induced by LRG1 and total T cells were not affected (figure 5K and online supplemental figure S7G,H).

Blocking GSK3A enhances the therapeutic efficacy of anti-PD-1 monoclonal antibody treatment

Immunohistochemical staining on a tissue microarray containing 23 patients with HCC samples collected from Huashan Hospital was performed (figure 6A). The results showed that GSK3A was positively correlated with LRG1, MPO, CitH3, and GZMB, but not associated with CD8$^+$ T-cell infiltration (figure 6B). Transcriptomic data from the TCGA database confirmed that both low expression of *GSK3A* and NETs-score had the best prognosis (figure 6C).

Furthermore, we assessed whether the expression of GSK3A in HCC would impact the efficacy of ICIs. Tumorous GSK3A and NETs level were tested in another cohort of 32 patients with HCC who received anti-PD-1 therapy, which were divided into two groups based on their response to anti-PD-1 therapy (figure 6D). The expression of GSK3A and NETs were synchronously increased in the non-responder group (GSK3A:9/13, NETs:11/13) compared with the responder group (GSK3A:5/19, NETs: 6/19) (figure 6E–G).

We performed combination therapy using a GSK3A inhibitor (SB216763) and anti-PD-1 antibody in Hepa1-6 orthotopic HCC model.[25 26] Combination treatment exhibited significant reduction or even disappearance of tumor volume (figure 6H). Flow cytometric analysis revealed that the combination significantly enhanced the cytotoxic activity of CTLs (figure 6I). The dual anti-tumor effect of GSK3A inhibitor and anti-PD-1 was validated in another *Gsk3a* expressing spontaneous murine hydrodynamic HCC model (figure 6J and online supplemental figure S7I). In conclusion, our findings suggested that inhibition of GSK3A could enhance the efficacy of anti-PD-1 therapy, serving as a new target to broaden the potential population for ICIs therapy in HCC.

DISCUSSION

Despite the significant success of immunotherapy, represented by ICIs, its efficacy in patients with HCC appears to be unsatisfactory.[27] To explore the complex interplay between HCC cells and the immune system and identify new immunotherapeutic targets, we employed in vivo CRISPR screening based on a mouse disease-relevant immune gene library. By applying immune selection pressure on immunocompetent and immunodeficient mice, we identified key genes that regulate HCC cell immune

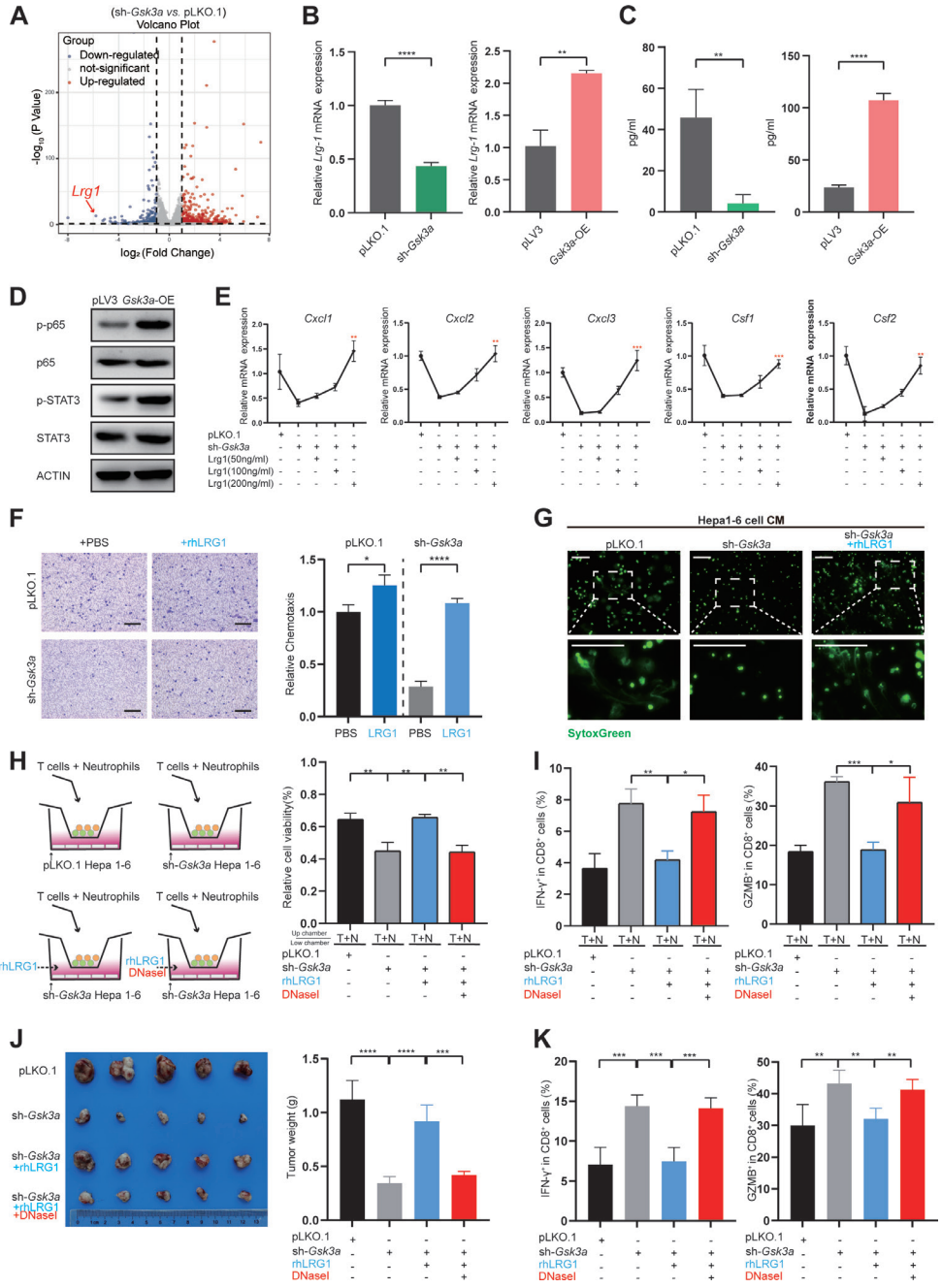

Figure 5 *Gsk3a* promotes recruitment and NETs formation of neutrophil through LRG1. (A) The volcano plot of differentially expressed genes in sh-*Gsk3a* versus pLKO.1 Hepa1-6 cells. (B) qPCR validation of the differentially expressed gene *Lrg1* in Hepa1-6 cells. (C) ELISA validation of LRG1 protein expression in Hepa1-6 cell culture supernatant. (D) Western blot validation of *Gsk3a* phosphorylation on the NFκB pathway and STAT3 pathway. (E) qPCR validation showed a concentration-dependent upregulation of chemokine expression (*Cxcl1*, *Cxcl2*, *Cxcl3*, *Csf1*, *Csf2*) with the supplementation of exogenous LRG1 protein. (F) Transwell assays demonstrated that reconstitution with recombinant LRG1 protein restored the reduced neutrophil chemotaxis caused by *Gsk3a* knockdown. Scare bar: 100 µm. (G) The representative immunofluorescence images showed that reconstitution with recombinant LRG1 protein restored the reduced NETs formation caused by *Gsk3a* knockdown. Scare bar: 100 µm. (H) The viability of sh-*Gsk3a* Hepa1-6 cells in the co-culture system of neutrophils and $CD8^+$ T cells with recombinant LRG1 protein or combined DNase I treatment. (I) Flow cytometric analysis of the frequency of IFN-γ^+ cells in $CD8^+$ T cells and $GZMB^+$ cells in $CD8^+$ T cells from the lower chamber after treatment with recombinant LRG1 protein or combined DNase I treatment. (J) In vitro images of sh-*Gsk3a* Hepa1-6 subcutaneous tumors in C57BL/6 mice treated with recombinant LRG1 protein or in combination with DNase I. (K) Flow cytometric analysis of the frequency of IFN-γ^+ cells in $CD8^+$ T cells and $GZMB^+$ cells in $CD8^+$ T cells from tumor immune microenvironment. All data were presented as means±SD. *p<0.05; **p<0.01; ***p<0.001; ****p<0.0001; ns, p≥0.05.CM, conditioned media; qPCR, quantitative PCR; GZMB, granzyme B; IFN-γ, interferon-gamma; KO, knocked-down; LRG1, leucine-rich α-2-glycoprotein 1; mRNA, messenger RNA; NETs, neutrophil extracellular traps; OE, overexpressed; PBS, phosphate-buffered saline; NFκB, nuclear factor kappa B; STAT3, signal transducer and activator of transcription 3.

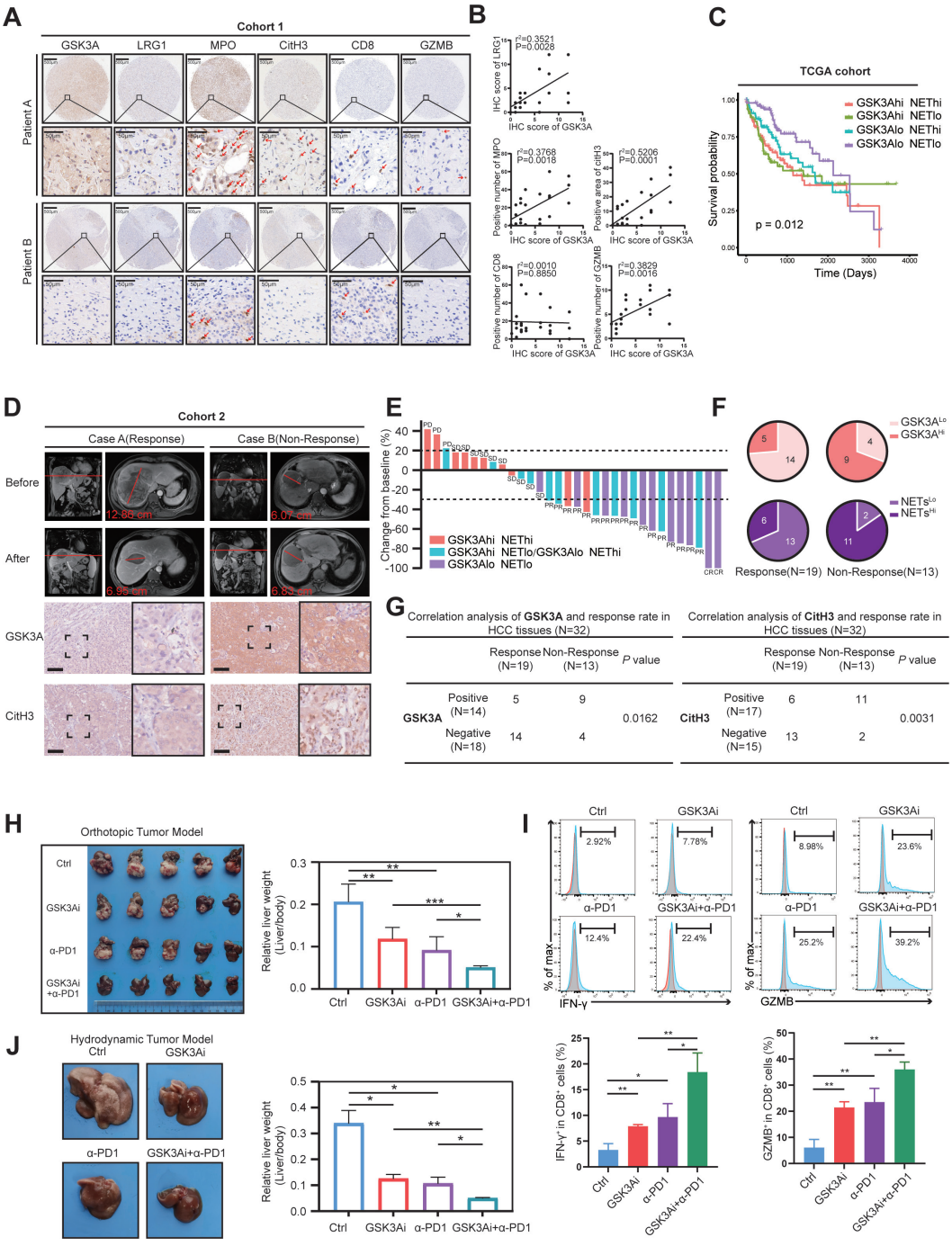

Figure 6 Blocking GSK3A enhances the therapeutic efficacy of anti-PD-1 monoclonal antibody treatment. (A) Representative images of immunohistochemical staining on the HCC tissue microarray. Scare bar:100 µm (up), 50 µm (down). (B) Correlations between GSK3A protein expression levels and scoring of LRG1, MPO, CitH3, CD8 and GZMB among samples from the HCC tissue microarray. (C) Prognostic analysis of patients based on high and low expression levels of *GSK3A* and NETs in TCGA cohort. (D) Representative MRI images of 32 patients before and after anti-PD-1 monoclonal antibody treatment (top). Representative IHC images of GSK3A and NETs expression. Scare bar: 100 µm (bottom). (E) Percentage change from baseline in sums of diameters of target lesions by modified Response Evaluation Criteria in Solid Tumors. (F) Pie charts of GSK3A and NETs expression in the anti-PD-1 monoclonal antibody treatment responsive and non-responsive groups after treatment. (G). The correlation between the expression of GSK3A and CitH3 and the reaction rate. P value by Fisher's exact probability test. (H) Ex vivo images and relative liver weight of Hepa1-6 orthotopic tumors treated with GSK3A inhibitor alone, anti-PD-1 monoclonal antibody alone, or their combination (n=5). (I) Flow cytometric analysis of the frequency of IFN-γ^+ cells in $CD8^+$ T cells and $GZMB^+$ cells in $CD8^+$ T cells isolated from C57BL/6 mice transplanted tumor in situ. (J) Ex vivo images and relative liver weight of hydrodynamic tumor model treated with GSK3A inhibitor alone, anti-PD-1 monoclonal antibody alone, or their combination (n=5). All data were presented as means±SD. *p<0.05; **p<0.01; ***p<0.001; ns, p≥0.05.GZMB, granzyme B; HCC, hepatocellular carcinoma; IFN-γ, interferon-gamma; IHC, immunohistochemistry; LRG1, leucine-rich α-2-glycoprotein 1; NETs, neutrophil extracellular traps; PD-1, programmed cell death protein-1; TCGA, The Cancer Genome Atlas.

adaptability. Through protein interaction analysis of immune evasion gene sets and in vivo/vitro validation, we successfully identified *Gsk3a* as a critical gene involved in HCC immune evasion. Our study reveals the involvement of *Gsk3a* in reshaping the tumor immune microenvironment, and pharmacological intervention targeting *Gsk3a* may enhance the sensitivity of immunotherapy.

Glycogen synthase kinase 3 (GSK-3), a serine/threonine kinase, plays critical roles in various diseases, including psychiatric and neurological disorders, inflammatory diseases, and cancer.[28] Through CRISPR screening, we identified and validated the critical role of *Gsk3a* in immune evasion in HCC; however, its functions between cancer and immunity remain unclear. In this study, we found that *Gsk3a* expression promoted tumor growth in immunocompetent mice but not in immunodeficient mice, suggesting its influence on tumor immune adaptability rather than intrinsic tumor growth. CTLs are central to the antitumor immune response, and the effector molecules produced on their activation play a crucial role in tumor killing. Flow cytometry analysis and transcriptomic sequencing also revealed the impact of *Gsk3a* on CTLs function rather than quantity. Additionally, *Gsk3a* expression positively correlated with neutrophil infiltration in the TME.

Both innate and adaptive immune surveillance play fundamental roles in the development of cancer and form the basis of various cancer immunotherapies.[29] HCC cells often induce an immune-suppressive microenvironment,[30 31] for example, through the modulation of Tregs,[32] tumor-associated macrophages,[33] and MDSCs,[34] leading to immune dysfunction. In recent years, the role of TANs in promoting HCC progression and metastasis has become an increasingly important topic of interest.[35 36] Growing evidence suggests that neutrophils are central to the pathogenesis of HCC, and extensive neutrophil infiltration in patients with HCC often indicates poorer outcomes.[37] Several studies have focused on the connection between neutrophils and immunosuppressive cells in the TME,[28 38] and neutrophils can suppress immune function by expressing PD-L1 and inducing T-cell apoptosis.[39–41] Our data suggest that *Gsk3a* inhibits $CD8^+$ T-cell function by promoting neutrophil infiltration in the TME, which has sparked our interest and highlights the important role of neutrophils in regulating HCC immune function. Furthermore, our research has confirmed the impact of *Gsk3a* on the expression profile of neutrophils, demonstrating that *Gsk3a* can influence the "quality" and "quantity" of neutrophils in the microenvironment by

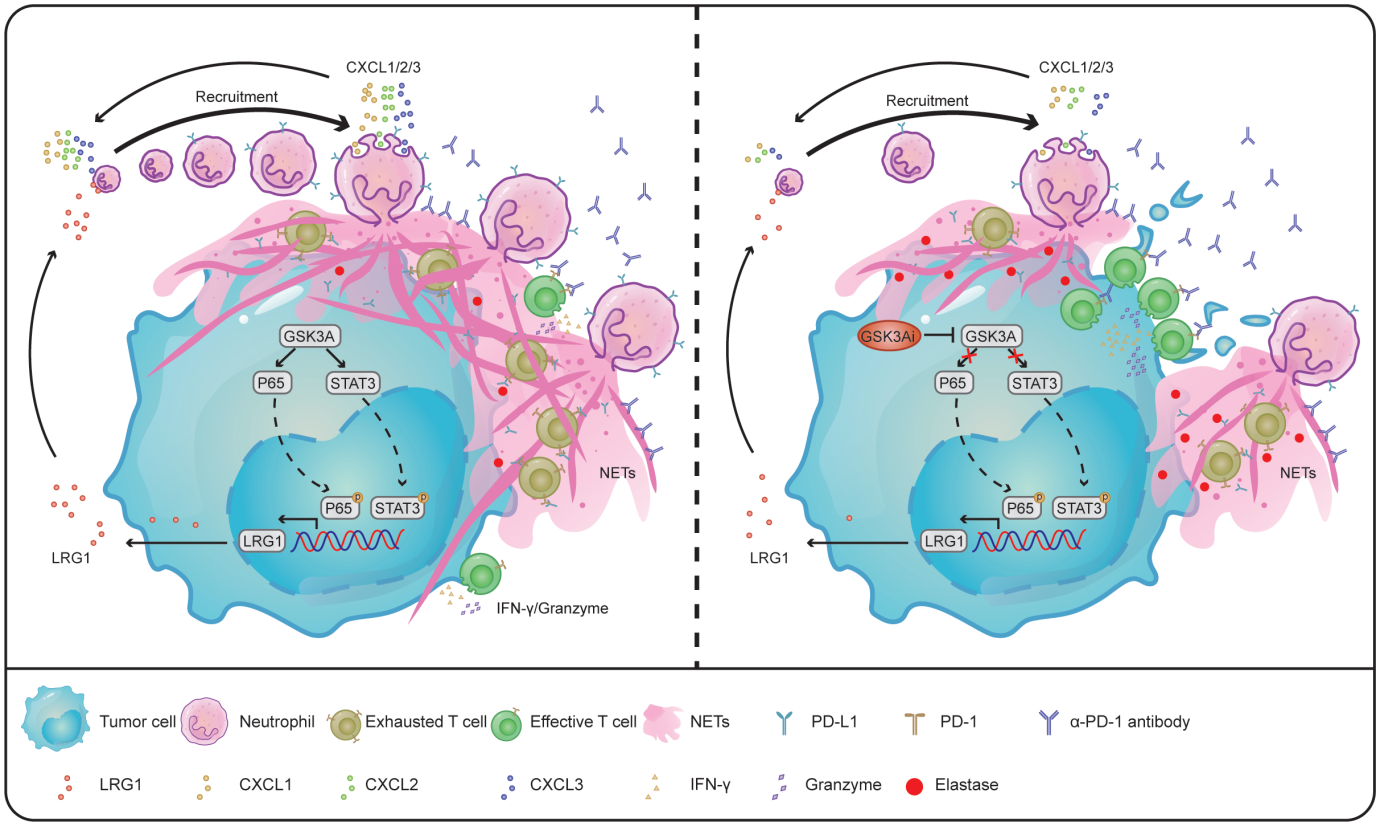

Figure 7 Schematic of GSK3A-induced immunosuppressive microenvironment formation. GSK3A upregulates the expression of LRG1 through the NF-κB/STAT3 axis, which induces neutrophil recruitment and the formation of immunosuppressive NETs. NETs induced by the GSK3A-LRG1 axis not only create physical barriers that block T-cell interaction with tumor cells, but also attenuate T-cell function by enriched PD-L1 expression within NETs. IFN-γ, interferon-gamma; LRG1, leucine-rich α-2-glycoprotein 1; NETs, neutrophil extracellular traps; PD-1, programmed cell death protein-1; PD-L1, programmed death-ligand 1; NFκB, nuclear factor kappa B; STAT3, signal transducer and activator of transcription 3.

promoting neutrophil positive autocrine chemotaxis and enhancing their immunosuppressive characteristics.

NETs are web-like structures released by neutrophils in response to invading pathogens. Increasing evidence demonstrates the role of NETs in promoting tumor progression and facilitating tumor metastasis.[42–44] Our previous research revealed that pre-metastatic niches containing NETs can capture HCC cells and enhance the metastatic potential of tumors.[20] This sparked our interest in whether NETs in the primary tumor also influence the immune microenvironment of HCC, potentially aiding tumor escape from immune surveillance during the occurrence and development of tumors. Although some studies have reported immunosuppressive effects of NETs,[45 46] it remains unclear whether this phenomenon occurs in HCC. In our transcriptome sequencing analysis, we observed upregulation of the NETs-associated gene set, and subsequently, we validated the role of *Gsk3a* in promoting NET release by neutrophils in both in vitro and in vivo experiments. Our data also demonstrated that the physical barrier formed by NETs hindered the interaction between effector cells and tumor cells. Additionally, NET structures exhibited increased expression of the immune inhibitory molecule PD-L1. NETs inhibitor eliminated *Gsk3a*-induced T-cell functional differences.

Gsk3a is a kinase that regulates a multitude of downstream substrates.[47] Transcriptome analysis revealed that modulating *Gsk3a* expression significantly affected the secretion of the factor LRG1, while expression of other immune cell chemokines remained unchanged. LRG1, a secreted member of the leucine-rich repeat protein family, has been reported to modulate NETs formation and influence neutrophil function through autocrine regulation of L-selectin and CXCL-1 expression.[24 48 49] In this study, we confirmed the correlation between *Gsk3a* and *Lrg1* at both transcript and protein levels. Furthermore, we demonstrated that *Gsk3a* regulated the transcriptional level of *Lrg1* through NFκB/stat3 phosphorylation. Reconstitution of LRG1 restored the decreased neutrophil chemotaxis and NET formation abilities caused by *Gsk3a* knockdown, suggesting that *Lrg1* acts as a "bridge" mediating the effects of *Gsk3a* on neutrophil modulation.

Our findings have implications for guiding immunotherapy. In the clinical specimens collected at our institution, we found higher expression levels of *Gsk3a* and NETs in patients who did not respond to anti-PD-1 therapy compared with the responder group. TCGA data further demonstrated that the expression of GSK3A and NETs significantly affects the prognosis of patients with HCC. These findings suggest that the expression of *Gsk3a* may impact the efficacy of immunotherapy. Importantly, we observed that the combination of a pharmacological inhibitor targeting *Gsk3a* with anti-PD-1 monoclonal antibody significantly inhibited tumor growth and enhanced immune response in a murine orthotopic tumor model.

In conclusion, our study provides new potential therapeutic targets for HCC immunotherapy through a systematic and effective CRISPR screening approach. We elucidated the mechanistic role of the candidate target *Gsk3a*, which regulates neutrophil chemotaxis and the release of immunosuppressive NETs through the NFκB/STAT3-Lrg1 axis, resulting in the downregulation of T-cell function (figure 7). Our research may contribute to expanding the potential application of immune checkpoint inhibitors in a specific population.

Acknowledgements The authors would like to thank Ming Lu (Chinese Academy of Sciences, Shanghai) for providing the flow cytometry platform. We extend our thanks to all participants who contributed to this research.

Contributors XZ, LY, XS and JP are joint first authors. LY, L-XQ, LL and WZ designed the study. XZ, LY, XS and JP performed the experiments. YC, JC, HW and JM analyzed the data. ZC, SX, YL and BZ joined in the discussion. XZ and LY wrote the manuscript. L-XQ, LL and LY supervised the project. All authors have read and approved this article. LL, WZ and L-XQ responsible for the overall content as the guarantor.

Funding This work was funded by the national Nature Science Foundation of China (NO. 91959203, 82373017, 82072696, 82002532) and Shanghai "Rising Stars of Medical Talents" Youth Development Program: Youth Medical Talents – Specialist Program.

Competing interests None declared.

Patient consent for publication Not applicable.

Ethics approval This study involves human participants and was approved by The Ethics Committee of Huashan Hospital, Fudan University, ID: KY2023-1002. Participants gave informed consent to participate in the study before taking part.

Provenance and peer review Not commissioned; externally peer reviewed.

Data availability statement Data are available upon reasonable request.

ORCID iD
Xin Zheng http://orcid.org/0009-0000-7333-0287

REFERENCES

1 Llovet JM, Castet F, Heikenwalder M, *et al*. Immunotherapies for hepatocellular carcinoma. *Nat Rev Clin Oncol* 2022;19:151–72.
2 Dunn GP, Bruce AT, Ikeda H, *et al*. Cancer immunoediting: from immunosurveillance to tumor escape. *Nat Immunol* 2002;3:991–8.
3 Zheng C, Zheng L, Yoo J-K, *et al*. Landscape of Infiltrating T Cells in Liver Cancer Revealed by Single-Cell Sequencing. *Cell* 2017;169:1342–56.
4 Li Y, Wang W, Yang F, *et al*. The regulatory roles of neutrophils in adaptive immunity. *Cell Commun Signal* 2019;17:147.
5 Chtanova T, Schaeffer M, Han S-J, *et al*. Dynamics of neutrophil migration in lymph nodes during infection. *Immunity* 2008;29:487–96.
6 Ismail HF, Fick P, Zhang J, *et al*. Depletion of neutrophils in IL-10(-/-) mice delays clearance of gastric Helicobacter infection and decreases the Th1 immune response to Helicobacter. *J Immunol* 2003;170:3782–9.
7 Tillack K, Breiden P, Martin R, *et al*. T lymphocyte priming by neutrophil extracellular traps links innate and adaptive immune responses. *J Immunol* 2012;188:3150–9.

8 Llovet JM, Kelley RK, Villanueva A, *et al*. Hepatocellular carcinoma. *Nat Rev Dis Primers* 2021;7:6.
9 Larkin J, Chiarion-Sileni V, Gonzalez R, *et al*. Combined Nivolumab and Ipilimumab or Monotherapy in Untreated Melanoma. *N Engl J Med* 2015;373:23–34.
10 Motzer RJ, Escudier B, McDermott DF, *et al*. Nivolumab versus Everolimus in Advanced Renal-Cell Carcinoma. *N Engl J Med* 2015;373:1803–13.
11 Bellmunt J, de Wit R, Vaughn DJ, *et al*. Pembrolizumab as Second-Line Therapy for Advanced Urothelial Carcinoma. *N Engl J Med* 2017;376:1015–26.
12 Reck M, Rodríguez-Abreu D, Robinson AG, *et al*. Pembrolizumab versus Chemotherapy for PD-L1-Positive Non-Small-Cell Lung Cancer. *N Engl J Med* 2016;375:1823–33.
13 El-Khoueiry AB, Sangro B, Yau T, *et al*. Nivolumab in patients with advanced hepatocellular carcinoma (CheckMate 040): an open-label, non-comparative, phase 1/2 dose escalation and expansion trial. *Lancet* 2017;389:2492–502.
14 Zhu AX, Finn RS, Edeline J, *et al*. Pembrolizumab in patients with advanced hepatocellular carcinoma previously treated with sorafenib (KEYNOTE-224): a non-randomised, open-label phase 2 trial. *Lancet Oncol* 2018;19:940–52.
15 Shalem O, Sanjana NE, Hartenian E, *et al*. Genome-scale CRISPR-Cas9 knockout screening in human cells. *Science* 2014;343:84–7.
16 Manguso RT, Pope HW, Zimmer MD, *et al*. In vivo CRISPR screening identifies Ptpn2 as a cancer immunotherapy target. *Nature New Biol* 2017;547:413–8.
17 Wang X, Tokheim C, Gu SS, *et al*. Invivo CRISPR screens identify the E3 ligase Cop1 as a modulator of macrophage infiltration and cancer immunotherapy target. *Cell* 2021;184:5357–74.
18 Ji P, Gong Y, Jin M-L, *et al*. In vivo multidimensional CRISPR screens identify *Lgals2* as an immunotherapy target in triple-negative breast cancer. *Sci Adv* 2022;8:eabl8247.
19 Mehling R, Schwenck J, Lemberg C, *et al*. Immunomodulatory role of reactive oxygen species and nitrogen species during T cell-driven neutrophil-enriched acute and chronic cutaneous delayed-type hypersensitivity reactions. *Theranostics* 2021;11:470–90.
20 Yang L-Y, Luo Q, Lu L, *et al*. Increased neutrophil extracellular traps promote metastasis potential of hepatocellular carcinoma via provoking tumorous inflammatory response. *J Hematol Oncol* 2020;13:3.
21 Cui C, Chakraborty K, Tang XA, *et al*. Neutrophil elastase selectively kills cancer cells and attenuates tumorigenesis. *Cell* 2021;184:3163–77.
22 Hughes K, Wickenden JA, Allen JE, *et al*. Conditional deletion of Stat3 in mammary epithelium impairs the acute phase response and modulates immune cell numbers during post-lactational regression. *J Pathol* 2012;227:106–17.
23 Naka T, Fujimoto M. LRG is a novel inflammatory marker clinically useful for the evaluation of disease activity in rheumatoid arthritis and inflammatory bowel disease. *Immunol Med* 2018;41:62–7.
24 Yu B, Yang L, Song S, *et al*. LRG1 facilitates corneal fibrotic response by inducing neutrophil chemotaxis via Stat3 signaling in alkali-burned mouse corneas. *Am J Physiol Cell Physiol* 2021;321:C415–28.
25 Grassilli E, Ianzano L, Bonomo S, *et al*. GSK3A is redundant with GSK3B in modulating drug resistance and chemotherapy-induced necroptosis. *PLoS One* 2014;9:e100947.
26 Zhou J, Freeman TA, Ahmad F, *et al*. GSK-3α is a central regulator of age-related pathologies in mice. *J Clin Invest* 2013;123:64398:1821–32:.
27 Sperandio RC, Pestana RC, Miyamura BV, *et al*. Hepatocellular Carcinoma Immunotherapy. *Annu Rev Med* 2022;73:267–78.
28 Sionov RV, Fridlender ZG, Granot Z. The Multifaceted Roles Neutrophils Play in the Tumor Microenvironment. *Cancer Microenviron* 2015;8:125–58.
29 Pennock GK, Chow LQM. The Evolving Role of Immune Checkpoint Inhibitors in Cancer Treatment. *Oncologist* 2015;20:812–22.
30 Fu Y, Liu S, Zeng S, *et al*. From bench to bed: the tumor immune microenvironment and current immunotherapeutic strategies for hepatocellular carcinoma. *J Exp Clin Cancer Res* 2019;38:396.
31 Li X, Ramadori P, Pfister D, *et al*. The immunological and metabolic landscape in primary and metastatic liver cancer. *Nat Rev Cancer* 2021;21:541–57.
32 Suthen S, Lim CJ, Nguyen PHD, *et al*. Hypoxia-driven immunosuppression by Treg and type-2 conventional dendritic cells in HCC. *Hepatology* 2022;76:1329–44.
33 Chen J, Lin Z, Liu L, *et al*. GOLM1 exacerbates CD8+ T cell suppression in hepatocellular carcinoma by promoting exosomal PD-L1 transport into tumor-associated macrophages. *Sig Transduct Target Ther* 2021;6:397.
34 Xie M, Lin Z, Ji X, *et al*. FGF19/FGFR4-mediated elevation of ETV4 facilitates hepatocellular carcinoma metastasis by upregulating PD-L1 and CCL2. *J Hepatol* 2023;79:109–25.
35 Shaul ME, Fridlender ZG. Tumour-associated neutrophils in patients with cancer. *Nat Rev Clin Oncol* 2019;16:601–20.
36 Liu K, Wang FS, Xu R. Neutrophils in liver diseases: pathogenesis and therapeutic targets. *Cell Mol Immunol* 2021;18:38–44.
37 Personeni N, Giordano L, Abbadessa G, *et al*. Prognostic value of the neutrophil-to-lymphocyte ratio in the ARQ 197-215 second-line study for advanced hepatocellular carcinoma. *Oncotarget* 2017;8:14408–15.
38 Zhou S-L, Zhou Z-J, Hu Z-Q, *et al*. Tumor-Associated Neutrophils Recruit Macrophages and T-Regulatory Cells to Promote Progression of Hepatocellular Carcinoma and Resistance to Sorafenib. *Gastroenterology* 2016;150:1646–58.
39 He G, Zhang H, Zhou J, *et al*. Peritumoural neutrophils negatively regulate adaptive immunity via the PD-L1/PD-1 signalling pathway in hepatocellular carcinoma. *J Exp Clin Cancer Res* 2015;34:141.
40 Cheng Y, Li H, Deng Y, *et al*. Cancer-associated fibroblasts induce PDL1+ neutrophils through the IL6-STAT3 pathway that foster immune suppression in hepatocellular carcinoma. *Cell Death Dis* 2018;9:422.
41 Michaeli J, Shaul ME, Mishalian I, *et al*. Tumor-associated neutrophils induce apoptosis of non-activated CD8 T-cells in a TNFα and NO-dependent mechanism, promoting a tumor-supportive environment. *Oncoimmunology* 2017;6:e1356965.
42 Yang D, Liu J. Neutrophil Extracellular Traps: A New Player in Cancer Metastasis and Therapeutic Target. *J Exp Clin Cancer Res* 2021;40:233.
43 Demers M, Wong SL, Martinod K, *et al*. Priming of neutrophils toward NETosis promotes tumor growth. *Oncoimmunology* 2016;5:e1134073.
44 Park J, Wysocki RW, Amoozgar Z, *et al*. Cancer cells induce metastasis-supporting neutrophil extracellular DNA traps. *Sci Transl Med* 2016;8:361ra138.
45 Teijeira Á, Garasa S, Gato M, *et al*. CXCR1 and CXCR2 Chemokine Receptor Agonists Produced by Tumors Induce Neutrophil Extracellular Traps that Interfere with Immune Cytotoxicity. *Immunity* 2020;52:856–71.
46 Xia Y, He J, Zhang H, *et al*. AAV-mediated gene transfer of DNase I in the liver of mice with colorectal cancer reduces liver metastasis and restores local innate and adaptive immune response. *Mol Oncol* 2020;14:2920–35.
47 Beurel E, Grieco SF, Jope RS. Glycogen synthase kinase-3 (GSK3): regulation, actions, and diseases. *Pharmacol Ther* 2015;148:114–31.
48 Ai J, Druhan LJ, Hunter MG, *et al*. LRG-accelerated differentiation defines unique G-CSFR signaling pathways downstream of PU.1 and C/EBPepsilon that modulate neutrophil activation. *J Leukoc Biol* 2008;83:1277–85.
49 Liu C, Teo MHY, Pek SLT, *et al*. A Multifunctional Role of Leucine-Rich α-2-Glycoprotein 1 in Cutaneous Wound Healing Under Normal and Diabetic Conditions. *Diabetes* 2020;69:2467–80.